

1 **Pathogenicity, immunogenicity, and protective ability of an attenuated SARS-CoV-2**  
2 **variant with a deletion at the S1/S2 junction of the spike protein**

3

4 Pui Wang<sup>1</sup>, Siu-Ying Lau<sup>1</sup>, Shaofeng Deng<sup>1</sup>, Pin Chen<sup>1</sup>, Bobo Wing-Yee Mok<sup>1</sup>, Anna Jinxia  
5 Zhang<sup>1</sup>, Andrew Chak-Yiu Lee<sup>1</sup>, Kwok-Hung Chan<sup>1</sup>, Wenjun Song<sup>1,2</sup>, Kelvin Kai-Wang To<sup>1</sup>,  
6 Jasper Fuk-Woo Chan<sup>1</sup>, Kwok-Yung Yuen<sup>1</sup> and Honglin Chen<sup>1\*</sup>

7

8

9 <sup>1</sup>Department of Microbiology and State Key Laboratory for Emerging Infectious Diseases, Li  
10 Ka Shing Faculty of Medicine, The University of Hong Kong, Hong Kong SAR,

11 <sup>2</sup> State Key Laboratory of Respiratory Disease, Institute of Integration of Traditional and  
12 Western Medicine, The First Affiliated Hospital of Guangzhou Medical University,  
13 Guangzhou Medical University, 195 Dong Feng Road (W), Guangzhou 510180, China

14

15

16

17 **\*Correspondence to:** Honglin Chen, Department of Microbiology and State Key Laboratory  
18 for Emerging Infectious Diseases, Li Ka Shing Faculty of Medicine, The University of Hong  
19 Kong, Hong Kong SAR, China ([hlchen@hku.hk](mailto:hlchen@hku.hk))

20

21

22

23

24

25

26 **Abstract**

27 SARS-CoV-2 contains a PRRA polybasic cleavage motif considered critical for efficient  
28 infection and transmission in humans. We previously reported that virus variants with spike  
29 protein S1/S2 junction deletions spanning this motif are attenuated. Here we characterize a  
30 further cell-adapted SARS-CoV-2 variant, Ca-DelMut. Ca-DelMut replicates more efficiently  
31 than wild type or parental virus in cells, but causes no apparent disease in hamsters, despite  
32 replicating in respiratory tissues. Unlike wild type virus, Ca-DelMut does not induce  
33 proinflammatory cytokines in hamster infections, but still triggers a strong neutralizing  
34 antibody response. Ca-DelMut-immunized hamsters challenged with wild type SARS-CoV-2  
35 are fully protected, demonstrating sterilizing immunity.

36           The emergence of SARS-CoV-2, a novel zoonotic origin  $\beta$ -coronavirus, has led to the  
37 first documented pandemic caused by a coronavirus <sup>1,2</sup>. The virus continues to circulate  
38 globally in humans with rapidly increasing numbers of infections and casualties each day  
39 (<https://coronavirus.jhu.edu/map.html>). While coronaviruses from bats and pangolins have  
40 been found to be closely related to SARS-CoV-2 <sup>3-6</sup>, the direct ancestral virus which attained  
41 cross-species transmission and the intermediate animal host source of human infections have  
42 not been defined. In the past two decades, three coronaviruses have jumped the species  
43 barrier to infect humans <sup>7</sup>. SARS-CoV and MERS-CoV show limited human to human  
44 transmission ability while causing severe disease and mortality. In contrast, SARS-CoV-2,  
45 which uses the same human ACE2 binding receptor as SARS-CoV <sup>6</sup>, is highly transmissible  
46 and causes variable severity of disease, from asymptomatic infections to severe and fatal  
47 outcomes. Analysis of the SARS-CoV-2 genome reveals a distinct PRRA polybasic cleavage  
48 motif at the S1/S2 junction of the spike protein when compared to the most proximal animal  
49 coronaviruses yet detected <sup>8</sup>. Cleavage of spike into S1 and S2 subunits by the cellular  
50 protease furin promotes cell fusion mediated by S2, which is critical for cellular entry of  
51 coronavirus<sup>9 10</sup>. In avian influenza virus, acquisition of a polybasic cleavage motif facilitates  
52 infection of an increased variety of cell types <sup>11-13</sup>. This polybasic cleavage site is essential  
53 for infection of human lung cells <sup>14</sup>. It is speculated that acquisition of the PRRA polybasic  
54 motif in the spike protein of SARS-CoV-2 provides the virus with its unique ability of cross  
55 species transmission; this motif therefore appears to serve as a pathogenic element in human  
56 infections <sup>10,14</sup>. If the PRRA polybasic cleavage motif was not a natural functional component  
57 in the original virus and acquired after cross species transmission, it is postulated that it may  
58 not be stable during the infection of its new hosts, or may need further adaptation. Indeed, a  
59 panel of SARS-CoV-2 variants with various lengths of deletion spanning the PRRA  
60 polybasic cleavage motif at the spike protein S1/S2 junction were identified in cultured cells

61 and at low levels in clinical specimens, suggesting the S1/S2 junction may be under selection  
62 pressure as the SARS-CoV-2 virus circulates in humans <sup>15,16</sup>. Initial characterization revealed  
63 that deletion at the S1/S2 junction causes SARS-CoV-2 virus attenuation in hamsters and  
64 prompted a further study to understand the properties of these deletion mutants in *in vitro* and  
65 *in vivo* systems. It remains to be determined whether some of these deletion variants may  
66 become more prevalent in humans as their circulation continues. On the other hand, these  
67 attenuated SARS-CoV-2 variants may hold promise as candidate live vaccines and it is  
68 important that their potential in this regard be evaluated.

69 To understand the role of the polybasic cleavage site in the infection and replication  
70 of SARS-CoV-2 and determine the stability of deletion variants, a previously characterized  
71 deletion mutant <sup>15</sup>, Del-Mut-1, was further adapted in Vero cells to obtain a highly attenuated  
72 variant of SARS-CoV-2 virus, designated Ca-DelMut. We analyzed the growth properties of  
73 this variant in cells and evaluated its pathogenicity in a hamster model. While it is attenuated  
74 in the ability to cause disease in animals, Ca-DelMut replicates to a higher titer in Vero cells  
75 than the wild type SARS-CoV-2 virus. High titers of neutralizing antibodies were detected in  
76 animals previously infected with Ca-DelMut variant. However, infection with Ca-DelMut  
77 does not induce the high levels of proinflammatory cytokines seen in wild type virus  
78 infections. Importantly, Ca-DelMut immunized hamsters showed full protection with  
79 sterilizing immunity against challenge with two different strains of wild type virus.

80

## 81 **Results**

### 82 **Growth and pathogenic properties of Ca-DelMut *in vitro* and *in vivo***

83 We previously identified and characterized a panel of SARS-CoV-2 variants  
84 containing 15-30bp deletions at the S1/S2 junction of the spike protein. One of the variants,  
85 Del-Mut-1, which contains a 30bp deletion spanning the PRRA polybasic cleavage motif was  
86 shown to be attenuated in a hamster infection model <sup>15</sup>. We further passaged this mutant in  
87 Vero E6 cells and obtained a variant with additional mutations in multiple genes in the  
88 background of Del-Mut-1, designated Ca-DelMut (**Figure 1 and Supplementary Table 1**).  
89 Growth properties of Ca-DelMut, parental Del-Mut-1 and a wild type (HK-13) SARS-CoV-2  
90 were analyzed in Vero E6 and Calu-3 cells. It is interesting to note that in Vero E6 cells both  
91 Del-Mut-1 and Ca-DelMut grow to a significantly higher titer at the 24 and 48-hour time  
92 points than the wild type virus, with Ca-DelMut showing the strongest growth ability in both  
93 cell types (**Figure 2A**). Notably, Ca-DelMut exhibits a cold adaptation phenotype *in vitro*, as  
94 demonstrated by comparatively high level of replication at 30°C, whereas wild type virus  
95 (HK-13) replicates poorly at this temperature (**Figure S1**). Attenuation of Del-Mut-1 was  
96 reported previously <sup>15</sup>. To further characterize the Ca-DelMut variant of SARS-CoV-2, we  
97 infected hamsters with variant and wild type SARS-CoV-2 strains. While inoculation with  
98 10<sup>3</sup> pfu HK-13 caused significant body weight loss post-infection, no apparent body weight  
99 loss was observed in Ca-DelMut (1.25x10<sup>5</sup> and 10<sup>3</sup> pfu) infected hamsters (**Figure 2B**).  
100 Histopathological analysis showed only mild regional alveolar septal infiltration and blood  
101 vessel congestion, with no obvious bronchiolar epithelium desquamation or luminal debris,  
102 no alveolar space infiltration or exudation, and no pathological changes in the intestines of  
103 Ca-DelMut infected hamsters, which are markedly different from the severe pathology  
104 observed in wild type virus infected animals (**Figure S2**). Examination of virus replication in  
105 lung and nasal turbinate tissues showed that Ca-DelMut replicates actively in the nasal

106 turbinate tissues but that replication efficiency is much lower than that of HK-13 in hamster  
107 lungs (**Figure 2C**). These results indicate that Ca-DelMut has altered tissue tropism and is  
108 more likely to infect and replicate in the upper respiratory tract.

### 109 **Immune response to infection with Ca-DelMut in hamsters**

110 Impaired or dysfunctional immune responses have been characterized as an important  
111 mechanism of pathogenesis in human SARS-CoV-2 infections<sup>17-19</sup>. Research on SARS-CoV  
112 and MERS-CoV has revealed that the interferon-mediated antiviral response is a double-  
113 edged sword which can induce both protective and pathogenic effects in humans. How Ca-  
114 DelMut infection induces the host immune response is of interest for understanding the  
115 molecular basis of its attenuation. To test if infection with Ca-DelMut may induce a different  
116 immune response from that elicited by wild type SARS-CoV-2, we examined interferon and  
117 cytokine expression in the lung tissues of virus infected hamsters. In contrast to infection  
118 with wild type HK-13 strain, we found that the Ca-DelMut variant does not provoke elevated  
119 levels of cytokines in infected hamsters (**Figure 3 and S3**). Aberrant activation of IL6 has  
120 been recognized as an important biomarker of disease severity in SARS-CoV-2 infected  
121 patients<sup>19-21</sup>. Remarkably, activation of IL-6 was only observed in HK-13 strain infected  
122 hamsters but not in those infected with Ca-DelMut variant. We then analyzed the adaptive  
123 immune response in hamsters previously infected with Ca-DelMut or wild type virus. Levels  
124 of receptor binding domain (RBD) specific antibodies in sera collected three weeks after  
125 infection were determined. Sera from both hamsters previously infected with Ca-DelMut or  
126 that had recovered from wild type virus (HK-13)<sup>22</sup> infection showed robust induction of  
127 RBD specific antibodies (**Figure 4A and S4A**). Cell based neutralization assays also  
128 demonstrated strong neutralizing activity against the wild type virus strain HK-13 in sera  
129 collected from both Ca-DelMut variant and wild type SARS-CoV-2 virus (HK-13) infected  
130 hamsters (**Figure 4B and S4B**). These results indicate that infection with Ca-DelMut leads to

131 an altered immune response which does not induce the elevated levels of proinflammatory  
132 cytokines seen in wild type SARS-CoV-2 virus infection. Nonetheless Ca-DelMut elicits a  
133 strong adaptive immune response, as demonstrated by robust neutralizing antibody  
134 production.

135 **Infection with Ca-DelMut confers full protection against SARS-CoV-2 infection with**  
136 **sterilizing immunity**

137 Because infection with Ca-DelMut causes no apparent disease in hamsters while  
138 inducing a strong neutralizing antibody response, we examined the potential of Ca-DelMut as  
139 a live attenuated virus vaccine to prevent SARS-CoV-2 virus infection and disease. Four  
140 weeks after infection with Ca-DelMut live attenuated virus, hamsters were re-challenged with  
141 wild type SARS-CoV-2 viruses. Two strains of SARS-CoV-2, HK-13 and HK-95, were used  
142 in the challenge experiment. HK-95 contains a D614G substitution in the spike protein,  
143 which has been suggested to bestow SARS-CoV-2 with higher infectivity in humans <sup>23</sup>.  
144 Negligible body weight loss was observed in Ca-DelMut vaccinated hamsters infected with  
145 either strain of wild type virus, whereas control hamsters not immunized with Ca-DelMut lost  
146 about 12-15 percent of body weight by day 5 post-infection (**Figure 5A and S5**). Analyses of  
147 virus replication in the lung and nasal turbinate tissues of re-challenged hamsters showed that  
148 Ca-DelMut infection provides sterilizing immunity against subsequent challenge with either  
149 HK-13 or HK-95 SARS-CoV-2, with the quantity of virus being either very low or below the  
150 level of detection in both lung and nasal tissues on days 2 and 5 post-infection (**Figure 5B**  
151 **and S5**). Histopathological analysis showed that mock-vaccinated hamster lungs collected at  
152 day 5 post-infection with either wild type virus strain showed extensive alveolar exudation  
153 and infiltration; bronchiolar epithelial cell death with luminal exudation and cell debris were  
154 also observed (**Figure 6**). In contrast, Ca-DelMut inoculated hamsters challenged with either  
155 strain of wild type SARS-CoV-2 virus only experienced mild regional alveolar septal

156 infiltration and blood vessel congestion at days 2 and 5 post-infection. No other pulmonary  
157 histopathological changes were observed. Our experiment also showed a lower inoculum of  
158 Ca-DelMut ( $1 \times 10^3$  pfu) is sufficient to provide full protection to the wild type virus  
159 challenge (**Figure S6**). These data indicate that prior infection with live attenuated Ca-  
160 DelMut variant virus provides complete protection against infection with wild type SARS-  
161 CoV-2 viruses in hamsters.

162

163



164 **Discussion**

165           Coronaviruses are zoonotic pathogens with distinct cross species transmissibility <sup>24</sup>.  
166 Besides 229E, OC43, HKU-1 and NL63, which have long been circulating in humans,  
167 SARS-CoV, MERS-CoV and SARS-CoV-2 have jumped the species barrier to infect humans  
168 in recent years <sup>7</sup>. SARS-CoV disappeared in 2004, while MERS-CoV is restricted to a few  
169 countries in the Middle East with only sporadic human transmissions since 2012 <sup>25</sup>. SARS-  
170 CoV-2 virus utilizes the same cellular receptor as SARS-CoV, ACE2, for mediating human  
171 infection but has exhibited a distinctive infectivity and transmissibility profile since it was  
172 first recognized in humans in Wuhan, China, in December 2019 <sup>6</sup>. There is strong interest in  
173 understanding how SARS-CoV-2 has acquired the unique ability to infect and transmit  
174 efficiently in humans. SARS-CoV-2 contains a PRRA polybasic motif not seen in the most  
175 closely related bat and pangolin coronaviruses currently known <sup>3,5,8</sup>. The presence of a  
176 polybasic cleavage site at the S1/S2 junction of the spike protein of SARS-CoV-2 virus is  
177 considered a critical property for enhanced coronavirus infectivity in humans and zoonotic  
178 potential <sup>14,26</sup>. A peptide assay has shown that the polybasic cleavage site harbored in SARS-  
179 CoV-2 is more accessible to proteases which activate the coronavirus spike protein <sup>10</sup>. If the  
180 polybasic cleavage site is one of the essential elements providing SARS-CoV-2 with  
181 increased infectivity and pathogenicity in humans, removal of this determinant could  
182 logically attenuate SARS-CoV-2 into a mild respiratory virus similar to the less pathogenic  
183 common coronaviruses currently circulating. Our previous report on a panel of attenuated  
184 variants with deletions at the S1/S2 junction supports this contention <sup>15</sup>. This study has  
185 further characterized one such mutant, Ca-DelMut, showing that it has low pathogenicity and  
186 does not provoke an inflammatory response in hamsters and that it induces adaptive  
187 immunity protective against subsequent infection with more pathogenic SARS-CoV-2 strains.

188 Ca-DelMut attenuated virus could also be a useful tool for studying SARS-CoV-2 replication,  
189 host tissue tropism and transmissibility.

190 Although both SARS-CoV and SARS-CoV-2 utilize ACE2 to mediate infection, the  
191 distinctive infectivity and pathogenicity displayed by SARS-CoV-2 is likely to be associated  
192 with the acquisition of a polybasic furin cleavage site in the protein which, together with  
193 enhanced binding affinity of the SARS-CoV-2 RBD for ACE2, would significantly broaden  
194 the tissue tropism of this virus<sup>14,27</sup>. Deregulated innate immunity during the early stage of  
195 infection in the upper respiratory tract may determine the subsequent outcome of  
196 dissemination to the lower respiratory tract and disease severity<sup>17,28</sup>. We found that Ca-  
197 DelMut replicates to comparable levels to wild type virus in the nasal turbinates but less  
198 effectively than wild type virus in the lungs (**Figure 2C**). Importantly, while replication of  
199 Ca-DelMut variant was observed in lung tissues, the elevated expression of proinflammatory  
200 cytokines elicited in wild type virus infected hamsters was not detected (**Figure 3 and S3**).  
201 These observations clearly suggest that the polybasic cleavage motif is a virulence element in  
202 SARS-CoV-2 and that its removal makes SARS-CoV-2 much less pathogenic, and more  
203 similar to a common cold respiratory coronavirus. We believe that SARS-CoV-2 will  
204 continue to undergo further adaptation as it circulates in humans. Our previous study revealed  
205 that variants with deletions at the S1/S2 junction are present at low levels in clinical  
206 specimens<sup>16</sup>. In 2003, the SARS-like coronavirus characterized from civet cats and early-  
207 outbreak human SARS-CoV isolates contained a 29-bp sequence in the ORF8 sequence  
208 which was deleted following its subsequent circulation in humans<sup>29</sup>. Deletions in ORF7b and  
209 ORF8 have also been observed in SARS-CoV-2, although the significance of these  
210 alterations is currently unknown<sup>30,31</sup>. It remains to be seen if continued evolution of SARS-  
211 CoV-2 in humans will subsequently select for less pathogenic variants similar to Ca-DelMut,  
212 or with other mutations.

213           Several SARS-CoV-2 vaccines are being developed for use in humans<sup>32-35</sup>. However,  
214 no vaccine against a coronavirus has been developed before and there are concerns regarding  
215 whether current vaccine strategies will be able to provide adequate and sufficiently long  
216 lasting immunity to prevent infection and alleviate disease severity and spread. Anti-SARS-  
217 CoV-2 antibodies are reported to decline rapidly in naturally infected individuals<sup>36,37</sup>. This  
218 study showed that Ca-DelMut induces a different innate immune response to that observed in  
219 wild type virus infections in an animal model and evokes sterilizing protective adaptive  
220 immunity against challenge with wild type virus (Figure 4). Because Ca-DelMut is attenuated  
221 it does not provoke proinflammatory cytokines which could interfere with the induction of  
222 adaptive immunity. It is possible that the Ca-DelMut variant may be able to stimulate more  
223 balanced and long-lasting immunity; further study is required to comprehensively compare  
224 the immune profiles induced by Ca-DelMut and wild type SARS-CoV-2 viruses. The  
225 potential applications of this attenuated SARS-CoV-2 virus should be explored and evaluated.  
226 However, given the high replication efficiency and low pathogenicity of Ca-DelMut, it may  
227 be an ideal strain for production of an inactivated vaccine, in addition to holding promise as a  
228 live attenuated vaccine.  
229

## 230 **Online Methods**

### 231 **Generation of cell adapted Del-mut (Ca-DelMut) virus**

232 Del-mut viruses were prepared as previously described<sup>15</sup>. To generate Ca-DelMut virus, the  
233 Del-Mut-1 virus was serially passaged 10 times in Vero E6 cells at 33°C and then passaged at  
234 30°C 8 times. For each passage, incubation time was 2-3 days, depending on the occurrence  
235 of cytopathic effects. After the 18<sup>th</sup> passage, the virus was amplified in a T75 Flask, then  
236 titered by plaque assay and sequenced using the Sanger method.

### 237 **Growth kinetics**

238 Confluent Vero E6 or Calu-3 cells were infected at 0.01 moi with the indicated viruses and  
239 incubated for 3 days. Virus supernatant was collected at the indicated time points. Virus titers  
240 were determined by plaque assay using Vero E6 cells.

### 241 **Plaque assay**

242 Confluent Vero E6 cells in 6-well format were incubated with 10-fold serially diluted virus  
243 for 1 h. After adsorption, virus was discarded. Cells were washed and overlaid with 1%  
244 agarose in DMEM and incubated for 3 days at 37°C. Cells were fixed with 10%  
245 formaldehyde for 1 day. Agarose gels were then removed and plaques stained with 1%  
246 crystal violet and counted.

### 247 **Immunization and challenge of hamsters**

248 7-8 week old golden Syrian hamsters were anesthetized intraperitoneally with ketamine and  
249 xylazine and then immunized intranasally with  $1.25 \times 10^5$  pfu of Ca-DelMut or SZ-002 virus  
250 or mock immunized with PBS. Body weight and disease symptoms were monitored daily. At  
251 day 21, sera were collected from hamsters for anti-spike RBD IgG and neutralizing antibody  
252 determination. At day 28, Ca-DelMut- and mock-immunized hamsters were challenged with  
253 WT virus (HK-13 or HK-95) at a dose of  $1 \times 10^3$  pfu. Body weight and disease symptoms  
254 were monitored daily and at days 2 and 5, lung and nasal turbinate tissues were collected for

255 histopathology and virus titration by plaque assay. For low dose immunization, hamsters  
256 were immunized with  $10^3$  pfu of either Ca-DelMut or WT HK-13 virus, or mock immunized  
257 with PBS. All experiments involving SARS-CoV-2 were conducted in a biosafety level 3  
258 laboratory. All animal studies were approved by the Committee on the Use of Live Animals  
259 in Teaching and Research, The University of Hong Kong.

#### 260 **Pathogenicity of Ca-DelMut and wild type SARS-CoV-2 virus in hamsters**

261 Hamsters were challenged intranasally with  $1 \times 10^3$  or  $1.25 \times 10^5$  pfu of Ca-DelMut or  $1 \times 10^3$   
262 pfu of WT virus. Body weight and disease symptoms were monitored daily. At days 2 and 4,  
263 lung and nasal turbinate tissues were collected for histopathological study, determination of  
264 proinflammatory cytokine expression and virus titration.

#### 265 **Neutralization assay**

266 Heat inactivated sera from Ca-DelMut challenged hamsters were 2-fold serially diluted in  
267 DMEM medium and incubated with 100 pfu of the indicated virus at  $37^\circ\text{C}$  for 1 h. The mix  
268 was added to confluent Vero E6 cells and incubated for 4 days at  $37^\circ\text{C}$ . Naïve and WT  
269 challenged sera were used as controls. After 4 days, cytopathic effect (CPE) was detected by  
270 microscopy, with the neutralization endpoint being the highest serum dilution causing 50%  
271 inhibition of CPE.

#### 272 **ELISA**

273 A hamster anti-spike RBD IgG detection kit (Wantai-Bio) was used to detect RBD specific  
274 antibodies. Procedures were conducted in accordance with the manual. Briefly, heat  
275 inactivated sera from Ca-DelMut challenged hamsters were 10-fold serially diluted and added  
276 to the plate and incubated at  $37^\circ\text{C}$  for 30 mins. Sera from mock- and WT-challenged hamsters  
277 were included as controls. The plate was washed 5 times and then incubated with secondary  
278 antibody reagent at  $37^\circ\text{C}$  for 30 mins. After washing, color development solution was added

279 and the plate incubated at 37°C for 15 mins. Stop solution was added and absorbance at 450  
280 nm measured.

### 281 **Quantification of expression of proinflammatory cytokines and chemokines**

282 Expression of proinflammatory cytokines was quantified using a qRT-PCR technique similar  
283 to that described in a previous study<sup>38</sup>. Briefly, total RNA was extracted from hamster lungs  
284 using RNeasy RT reagent (MRC) according to the manual. cDNA was synthesized using a  
285 High Capacity cDNA Reverse Transcription Kit (Invitrogen) and oligo dT primers following  
286 the protocol provided. qPCR was performed using SYBR Premix Ex Taq (Takara) reagent  
287 and gene specific primers in an LC480 PCR machine (Roche). PCR conditions were as  
288 follows: initial denaturation: 95°C for 5 min, 45 cycles of amplification: 95°C for 10s, 60°C  
289 for 10s, 72°C for 10s, and melting curve analysis: 65°C to 97°C at 0.1°C/s. Expression of  
290 target genes was normalized to the internal reference gene (hamster  $\gamma$ -actin) and the  
291 comparative Ct ( $2^{-\Delta\Delta Ct}$ ) method utilized to calculate the cytokine expression profile.

### 292 **Histopathology**

293 Organs were fixed in 10% PBS buffered formalin and processed into paraffin-embedded  
294 blocks. Tissue sections were stained with haematoxylin and eosin (H&E) and examined by  
295 light microscopy as in a previous study<sup>38</sup>.

### 296 **Acknowledgements**

297 The authors would like to thank Dr Jane Rayner for critical reading and editing of the  
298 manuscript. This study is partly supported by the Theme-Based Research Scheme  
299 (T11/707/15) and General Research Fund (17107019) of the Research Grants Council, Hong  
300 Kong Special Administrative Region and the Sanming Project of Medicine in Shenzhen,  
301 China (No. SZSM201911014).

### 302 **Author Contributions**

303 P.W., and H.C. designed the studies, P.W., S-Y. L., S. D., P. C., B.W.M., A.J.Z., A.C-Y.L.,  
304 K-H.C. and W.S. performance experiments; P.W., S-Y. L., A. J. Z., K. K-W.T., J. F-W.C, K-  
305 Y. Y. and H.C. analyzed the data; P.W. and H.C. wrote the paper.

### 306 **Competing Interests statement**

307 The authors declare no conflict of interests.

308

### 309 **References**

- 310 1. Wu, F., *et al.* A new coronavirus associated with human respiratory disease in China. *Nature*  
311 **579**, 265-269 (2020).
- 312 2. Lu, R., *et al.* Genomic characterisation and epidemiology of 2019 novel coronavirus:  
313 implications for virus origins and receptor binding. *Lancet* **395**, 565-574 (2020).
- 314 3. Lam, T.T., *et al.* Identifying SARS-CoV-2-related coronaviruses in Malayan pangolins. *Nature*  
315 **583**, 282-285 (2020).
- 316 4. Zhang, T., Wu, Q. & Zhang, Z. Probable Pangolin Origin of SARS-CoV-2 Associated with the  
317 COVID-19 Outbreak. *Curr Biol* **30**, 1578 (2020).
- 318 5. Zhou, H., *et al.* A Novel Bat Coronavirus Closely Related to SARS-CoV-2 Contains Natural  
319 Insertions at the S1/S2 Cleavage Site of the Spike Protein. *Curr Biol* **30**, 2196-2203 e2193  
320 (2020).
- 321 6. Zhou, P., *et al.* A pneumonia outbreak associated with a new coronavirus of probable bat  
322 origin. *Nature* **579**, 270-273 (2020).
- 323 7. de Wit, E., van Doremalen, N., Falzarano, D. & Munster, V.J. SARS and MERS: recent insights  
324 into emerging coronaviruses. *Nat Rev Microbiol* **14**, 523-534 (2016).
- 325 8. Andersen, K.G., Rambaut, A., Lipkin, W.I., Holmes, E.C. & Garry, R.F. The proximal origin of  
326 SARS-CoV-2. *Nat Med* **26**, 450-452 (2020).
- 327 9. Matsuyama, S., Ujike, M., Morikawa, S., Tashiro, M. & Taguchi, F. Protease-mediated  
328 enhancement of severe acute respiratory syndrome coronavirus infection. *Proc Natl Acad Sci*  
329 *U S A* **102**, 12543-12547 (2005).
- 330 10. Jaimes, J.A., Millet, J.K. & Whittaker, G.R. Proteolytic Cleavage of the SARS-CoV-2 Spike  
331 Protein and the Role of the Novel S1/S2 Site. *iScience* **23**, 101212 (2020).
- 332 11. Kawaoka, Y. & Webster, R.G. Sequence requirements for cleavage activation of influenza  
333 virus hemagglutinin expressed in mammalian cells. *Proc Natl Acad Sci U S A* **85**, 324-328  
334 (1988).
- 335 12. Ito, T., *et al.* Generation of a highly pathogenic avian influenza A virus from an avirulent field  
336 isolate by passaging in chickens. *J Virol* **75**, 4439-4443 (2001).
- 337 13. Alexander, D.J. & Brown, I.H. History of highly pathogenic avian influenza. *Rev Sci Tech* **28**,  
338 19-38 (2009).
- 339 14. Hoffmann, M., Kleine-Weber, H. & Pohlmann, S. A Multibasic Cleavage Site in the Spike  
340 Protein of SARS-CoV-2 Is Essential for Infection of Human Lung Cells. *Mol Cell* **78**, 779-784  
341 e775 (2020).
- 342 15. Lau, S.Y., *et al.* Attenuated SARS-CoV-2 variants with deletions at the S1/S2 junction. *Emerg*  
343 *Microbes Infect* **9**, 837-842 (2020).
- 344 16. Wong, Y.C., *et al.* Natural transmission of bat-like SARS-CoV-2PRRA variants in COVID-19  
345 patients. *Clin Infect Dis* (2020).
- 346 17. Zhou, Z., *et al.* Heightened Innate Immune Responses in the Respiratory Tract of COVID-19  
347 Patients. *Cell Host Microbe* **27**, 883-890 e882 (2020).

- 348 18. Giamarellos-Bourboulis, E.J., *et al.* Complex Immune Dysregulation in COVID-19 Patients  
349 with Severe Respiratory Failure. *Cell Host Microbe* **27**, 992-1000 e1003 (2020).
- 350 19. Mazzone, A., *et al.* Impaired immune cell cytotoxicity in severe COVID-19 is IL-6 dependent. *J*  
351 *Clin Invest* (2020).
- 352 20. Chen, X., *et al.* Detectable serum SARS-CoV-2 viral load (RNAemia) is closely correlated with  
353 drastically elevated interleukin 6 (IL-6) level in critically ill COVID-19 patients. *Clin Infect Dis*  
354 (2020).
- 355 21. Luo, M., *et al.* IL-6 and CD8+ T cell counts combined are an early predictor of in-hospital  
356 mortality of patients with COVID-19. *JCI Insight* **5**(2020).
- 357 22. Chan, J.F., *et al.* A familial cluster of pneumonia associated with the 2019 novel coronavirus  
358 indicating person-to-person transmission: a study of a family cluster. *Lancet* **395**, 514-523  
359 (2020).
- 360 23. Korber, B., *et al.* Tracking Changes in SARS-CoV-2 Spike: Evidence that D614G Increases  
361 Infectivity of the COVID-19 Virus. *Cell* (2020).
- 362 24. Menachery, V.D., Graham, R.L. & Baric, R.S. Jumping species-a mechanism for coronavirus  
363 persistence and survival. *Curr Opin Virol* **23**, 1-7 (2017).
- 364 25. Chan, J.F., *et al.* Middle East respiratory syndrome coronavirus: another zoonotic  
365 betacoronavirus causing SARS-like disease. *Clin Microbiol Rev* **28**, 465-522 (2015).
- 366 26. Menachery, V.D., *et al.* Trypsin Treatment Unlocks Barrier for Zoonotic Bat Coronavirus  
367 Infection. *J Virol* **94**(2020).
- 368 27. Wrobel, A.G., *et al.* SARS-CoV-2 and bat RaTG13 spike glycoprotein structures inform on  
369 virus evolution and furin-cleavage effects. *Nat Struct Mol Biol* **27**, 763-767 (2020).
- 370 28. Hou, Y.J., *et al.* SARS-CoV-2 Reverse Genetics Reveals a Variable Infection Gradient in the  
371 Respiratory Tract. *Cell* **182**, 429-446 e414 (2020).
- 372 29. Guan, Y., *et al.* Isolation and characterization of viruses related to the SARS coronavirus from  
373 animals in southern China. *Science* **302**, 276-278 (2003).
- 374 30. Su, Y.C.F., *et al.* Discovery and Genomic Characterization of a 382-Nucleotide Deletion in  
375 ORF7b and ORF8 during the Early Evolution of SARS-CoV-2. *mBio* **11**(2020).
- 376 31. Gong, Y.N., *et al.* SARS-CoV-2 genomic surveillance in Taiwan revealed novel ORF8-deletion  
377 mutant and clade possibly associated with infections in Middle East. *Emerg Microbes Infect* **9**,  
378 1457-1466 (2020).
- 379 32. Gao, Q., *et al.* Development of an inactivated vaccine candidate for SARS-CoV-2. *Science* **369**,  
380 77-81 (2020).
- 381 33. Corbett, K.S., *et al.* Evaluation of the mRNA-1273 Vaccine against SARS-CoV-2 in Nonhuman  
382 Primates. *N Engl J Med* (2020).
- 383 34. Mercado, N.B., *et al.* Single-shot Ad26 vaccine protects against SARS-CoV-2 in rhesus  
384 macaques. *Nature* (2020).
- 385 35. Folegatti, P.M., *et al.* Safety and immunogenicity of the ChAdOx1 nCoV-19 vaccine against  
386 SARS-CoV-2: a preliminary report of a phase 1/2, single-blind, randomised controlled trial.  
387 *Lancet* (2020).
- 388 36. Long, Q.X., *et al.* Clinical and immunological assessment of asymptomatic SARS-CoV-2  
389 infections. *Nat Med* **26**, 1200-1204 (2020).
- 390 37. Yin, S., *et al.* Longitudinal anti-SARS-CoV-2 antibody profile and neutralization activity of a  
391 COVID-19 patient. *J Infect* **81**, e31-e32 (2020).
- 392 38. Chan, J.F., *et al.* Simulation of the clinical and pathological manifestations of Coronavirus  
393 Disease 2019 (COVID-19) in golden Syrian hamster model: implications for disease  
394 pathogenesis and transmissibility. *Clin Infect Dis* (2020).

395

396



397 **Figure legends**

398 **Figure 1. Schematic diagram of the SARS-CoV-2 genome showing the deletion and**

399 **mutations of Ca-DelMut.** Del-Mut-1 virus<sup>15</sup> was serially passaged in Vero E6 cells at 33°C

400 (10 passages) and 30°C (8 passages). Virus from the 18<sup>th</sup> passage was designated as Ca-

401 DelMut live attenuated SARS-CoV-2 virus and amplified to prepare a virus stock. Ca-

402 DelMut was sequenced by the Sanger method; mutations are shown in the diagram and in

403 Supplementary Table 1.

404 **Figure 2. Replication efficiency of Ca-DelMut *in vitro* and *in vivo*.** (A) Vero E6 or Calu-3

405 cells were infected with Ca-DelMut and other viruses at 0.01 moi and cultured at 37°C. At the

406 indicated time points, supernatants were collected, and virus titer determined by plaque assay

407 in Vero E6 cells. (B) Ca-DelMut infection in hamsters. Hamsters were infected intranasally

408 with either Ca-DelMut or wild type (WT) viruses at different doses, as indicated. Body

409 weight was monitored for 5 days. (C) Replication of Ca-DelMut in lung and nasal turbinate

410 tissues. After virus challenge ( $1 \times 10^3$  pfu), lung and nasal turbinate tissues were collected

411 from hamsters at days 2 and 4, then homogenized and virus titer determined. Error bars

412 represent mean  $\pm$  s.d. (n=3). Statistical comparisons between means were performed by

413 Student's t-test: \*\*\* p<0.001, \*\* p<0.01, \* p<0.05, NS: not significant.

414 **Figure 3. Proinflammatory cytokine response profiles in Ca-DelMut and wild type virus**

415 **infected hamsters.** Hamsters were infected intranasally with  $1 \times 10^3$  pfu of either Ca-DelMut

416 or WT HK-13 virus. At days 2 and 4, RNA was extracted from lung tissues of infected

417 hamsters and cDNA synthesized using oligo dT primers. Expression of different

418 proinflammatory cytokines was examined by qPCR, normalized to an internal reference gene

419 (hamster  $\gamma$ -actin), and the comparative Ct ( $2^{-\Delta\Delta Ct}$ ) method utilized to calculate the cytokine

420 expression profile. Statistical comparisons between means were performed by Student's t-test:

421 \*\*\*\* p<0.0001, \*\*\* p<0.001, \*\* p<0.01, \* p<0.05, ns: not significant.

422 **Figure 4. Antibodies induced by Ca-DelMut immunization of hamsters.** Hamsters were  
423 immunized intranasally with  $1.25 \times 10^5$  pfu of either Ca-DelMut or wild type virus (HK-001a)  
424 virus<sup>15,22</sup>, or mock immunized. At day 21, blood was collected from hamsters and tested for  
425 (A) anti-S1 RBD specific IgG titers and (B) neutralization activity against the HK-13 virus  
426 strain. Error bars represent mean  $\pm$  s.d. (n=3). LOD: level of detection. Statistical  
427 comparisons between means were performed by Student's t-test: \* p<0.05, ns: not significant

428 **Figure 5. Ca-DelMut immunization protection against WT virus challenge in hamsters.**  
429 Hamsters were inoculated with  $1.25 \times 10^5$  pfu Ca-DelMut or mock immunized. At day 28 after  
430 immunization, hamsters were challenged with  $1 \times 10^3$  pfu of either HK-13 or HK-95 virus. (A)  
431 Body weight and disease symptoms were monitored for 5 days. (B) At days 2 and 5 post-  
432 infection, lungs and nasal turbinate tissues were collected for virus titration and  
433 histopathological study. Error bars represent mean  $\pm$  s.d. (n=3).

434 **Figure 6. Histopathological analysis of lung pathology in WT virus challenged Ca-**  
435 **DelMut- and mock-immunized hamsters.** At day 28 after immunization, hamsters were  
436 challenged with  $1 \times 10^3$  pfu of either HK-13 or HK-95 virus. At days 2 and 5 post-infection,  
437 lungs were collected, fixed, processed into paraffin blocks and sections H&E stained.

438 (a) Challenge with HK-13. Day 2: Mock-vaccinated hamster lungs showed bronchiolar  
439 epithelial cell death and the bronchiolar lumen filled with exudate and cell debris (arrow).  
440 Diffuse alveolar infiltration and focal hemorrhage were also seen (arrowheads). Ca-DelMut-  
441 vaccinated hamster lungs showed regional alveolar septal infiltration and blood vessel  
442 congestion (arrowhead), but no obvious bronchiolar epithelial cell death (arrow). Day 5:  
443 Lungs of mock-vaccinated hamsters showed severe alveolar infiltration and exudation  
444 (arrowheads), as well as bronchiolar luminal exudation (arrow). Vaccinated hamster lungs  
445 showed focal alveolar septal infiltration (arrowheads), while the bronchiolar epithelium  
446 appeared normal with no luminal secretion or cell debris (arrows).

447 **(b)** Challenge with HK-95. Day 2: Mock-vaccinated hamster lungs showed bronchiolar  
448 epithelial cell death with luminal cell debris (arrow) and diffuse alveolar infiltration with  
449 focal hemorrhage and exudation (arrowheads), with a medium sized blood vessel showing  
450 severe endotheliitis (open arrow). Vaccinated hamster lungs showed regional alveolar septal  
451 infiltration and blood vessel congestion (arrowhead); a blood vessel appeared to be normal  
452 (open arrow), and no obvious bronchiolar epithelial cell death was observed (arrows). Day 5:  
453 Lungs of mock-vaccination control hamsters showed severe alveolar infiltration and  
454 exudation (arrowheads) and bronchiolar luminal cell debris (arrow). Vaccinated hamster  
455 lungs showed focal alveolar septal infiltration (arrowheads), while the bronchiolar epithelium  
456 appeared normal without luminal secretion (arrows). Scale bar: 100 $\mu$ m.

Figure 1

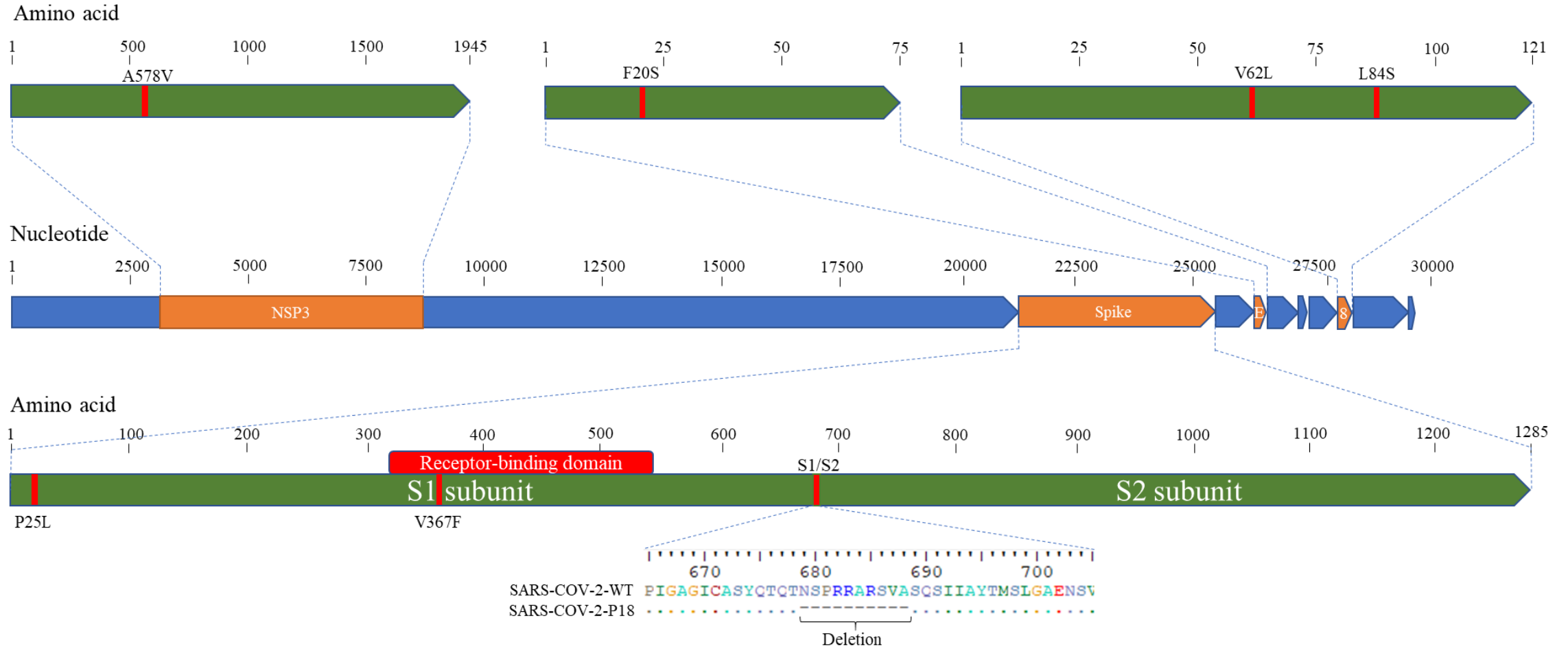
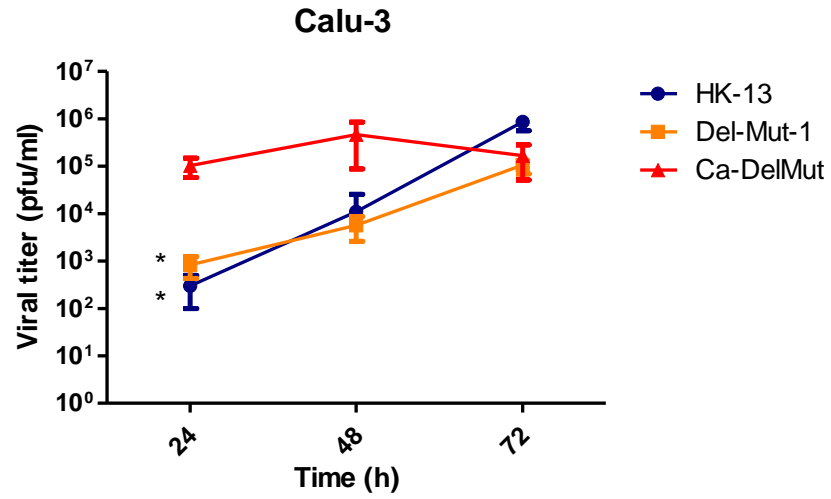
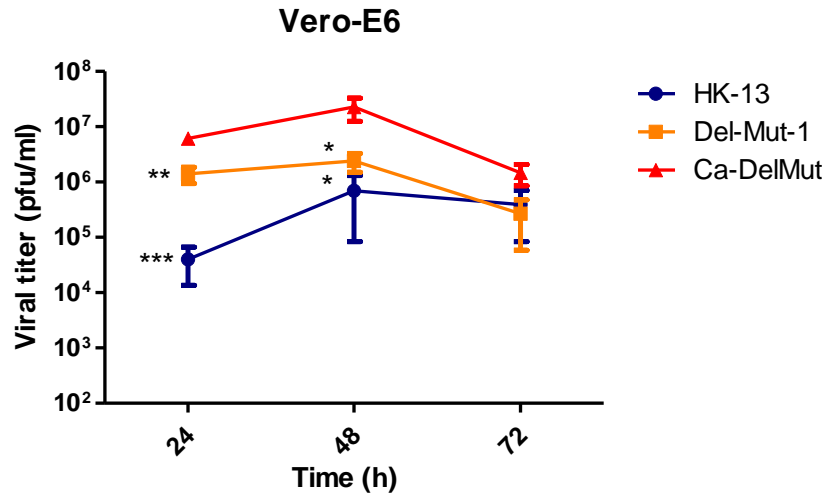
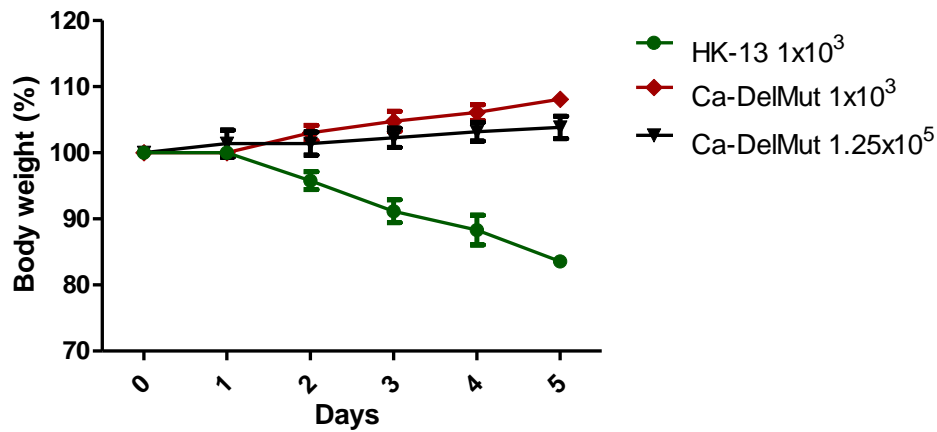


Figure 2

a



b



c

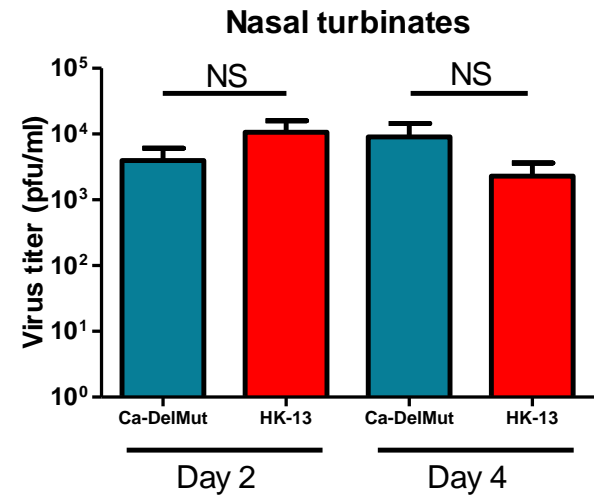
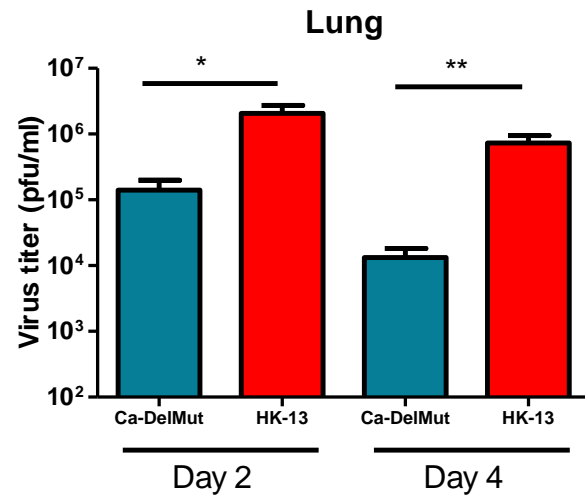


Figure 3

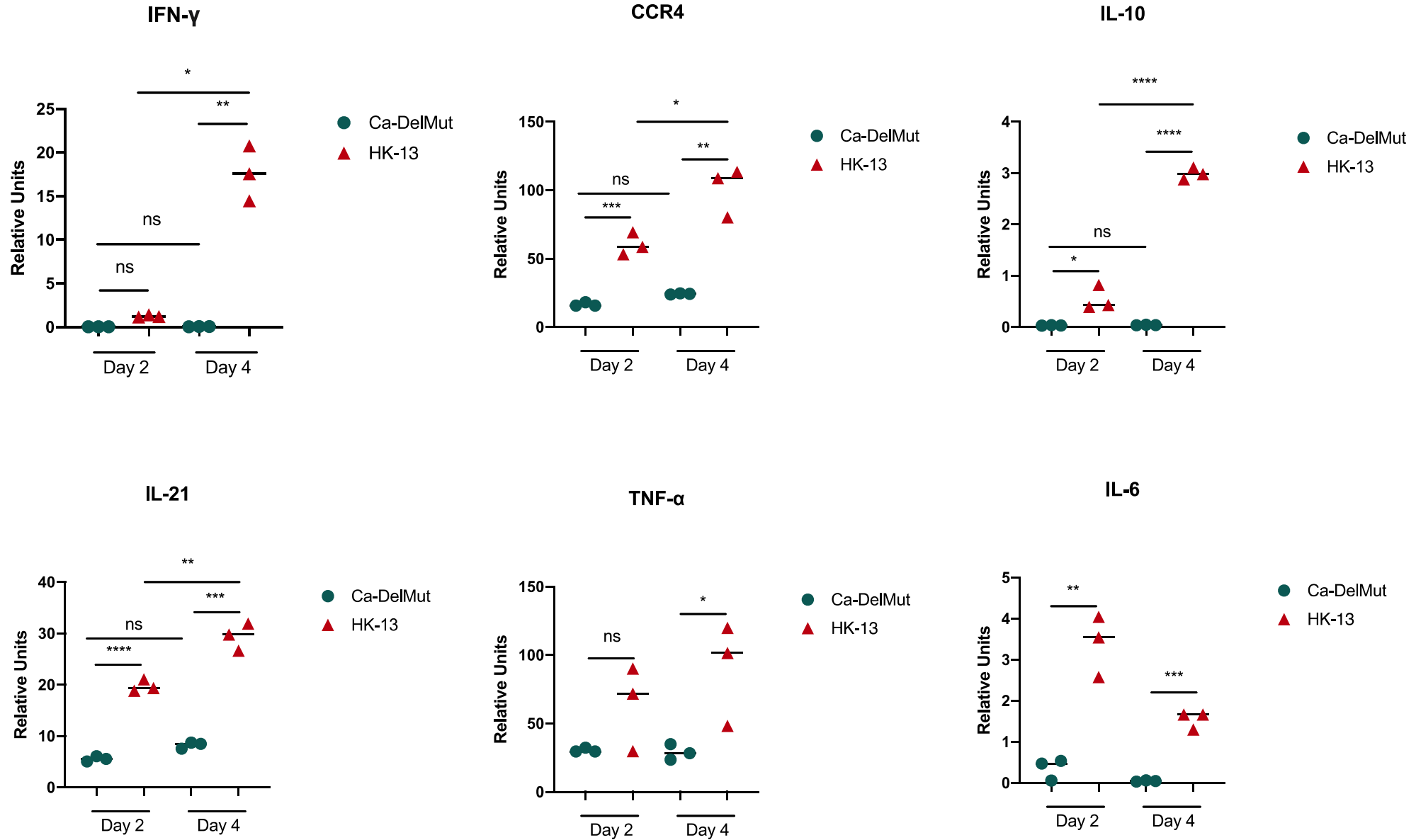
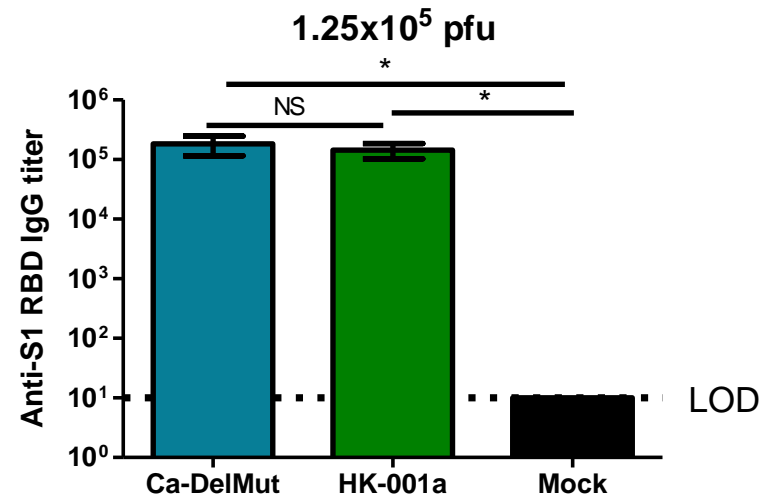


Figure 4

a



b

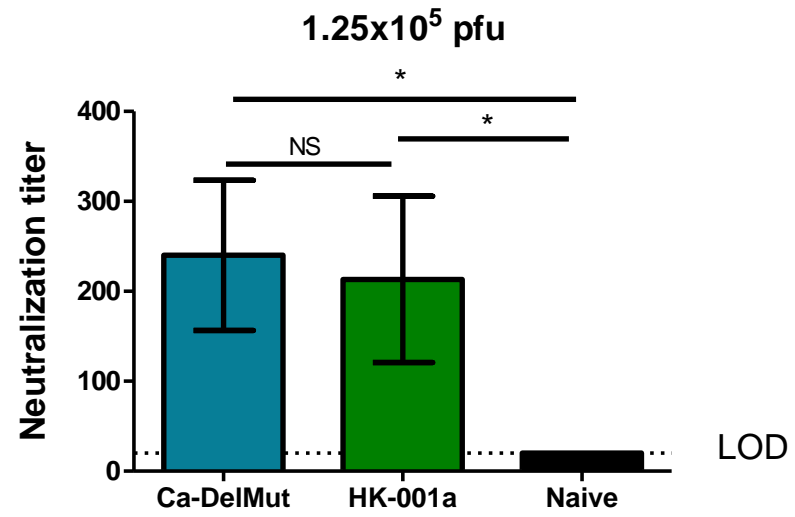
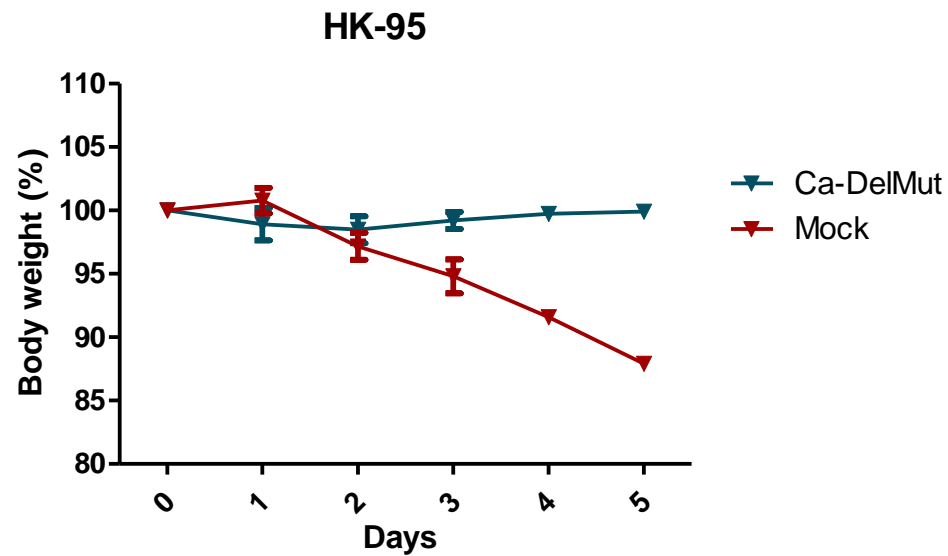
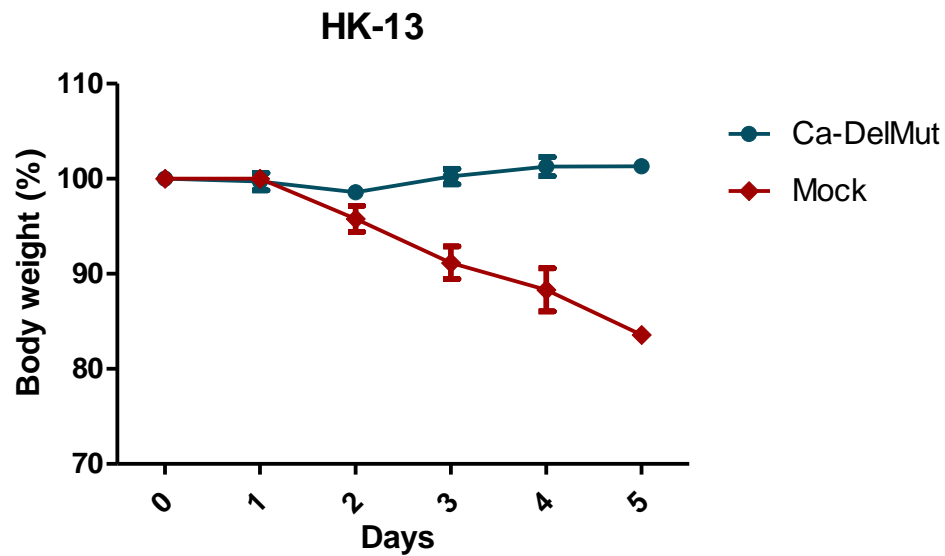
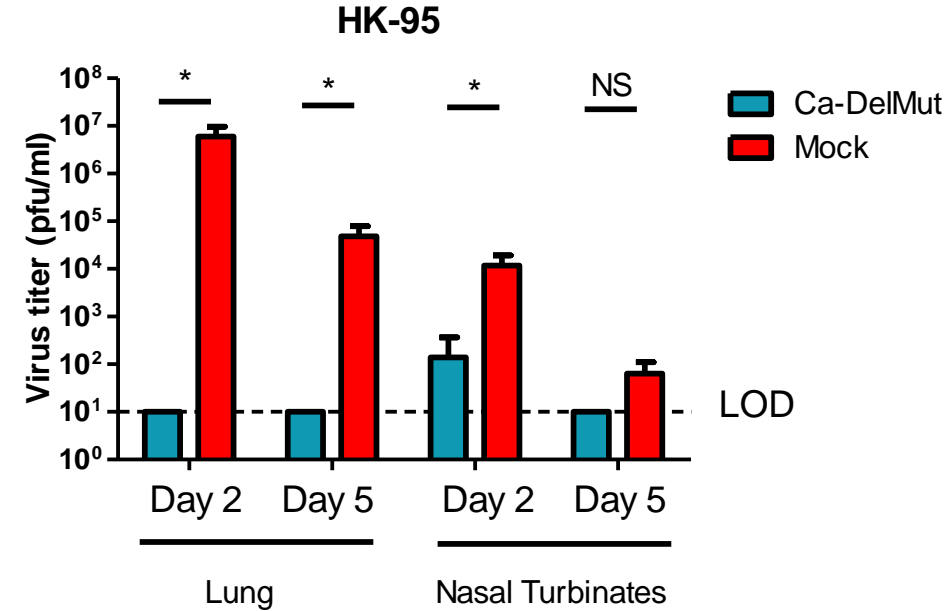
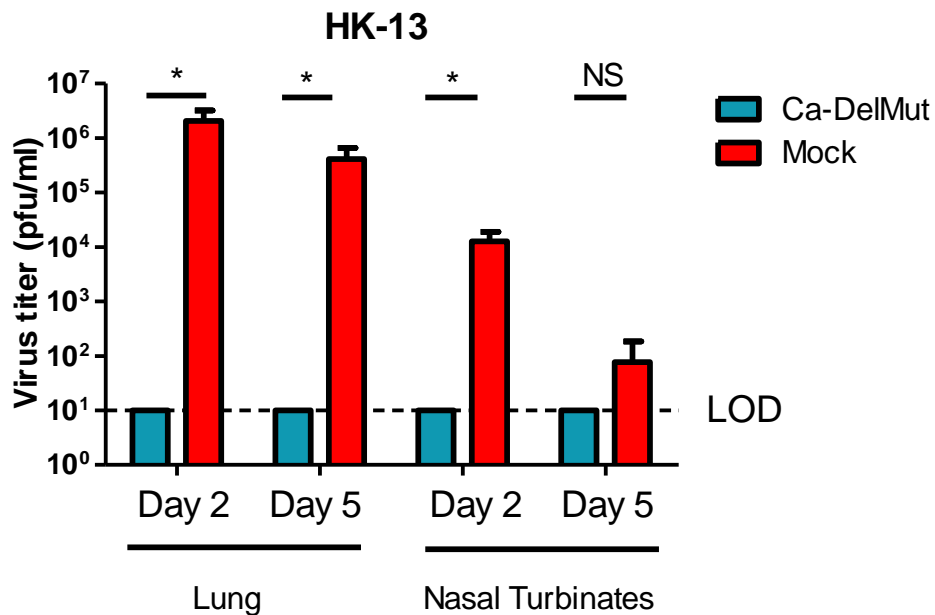


Figure 5

A

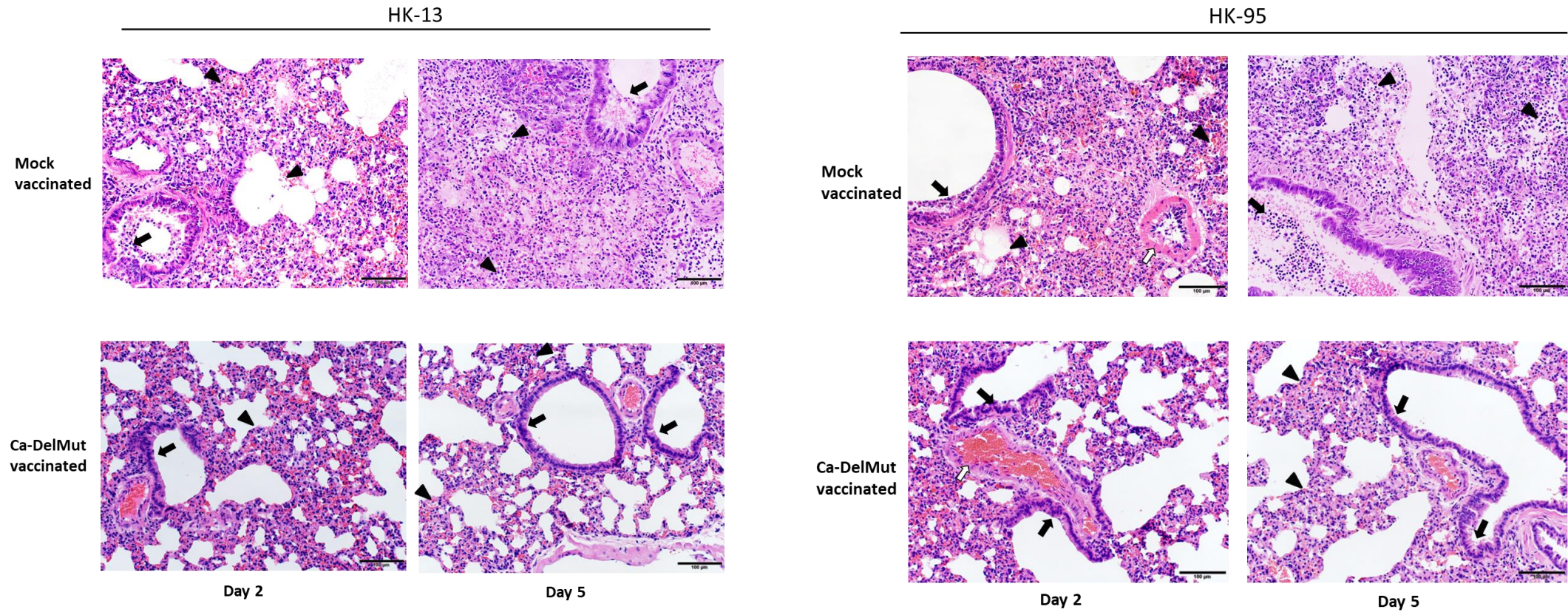


B





**Figure 6**



## Pathogenicity, immunogenicity, and protective ability of an attenuated SARS-CoV-2 variant with a deletion at the S1/S2 junction of the spike protein

### Supplementary Table 1\*

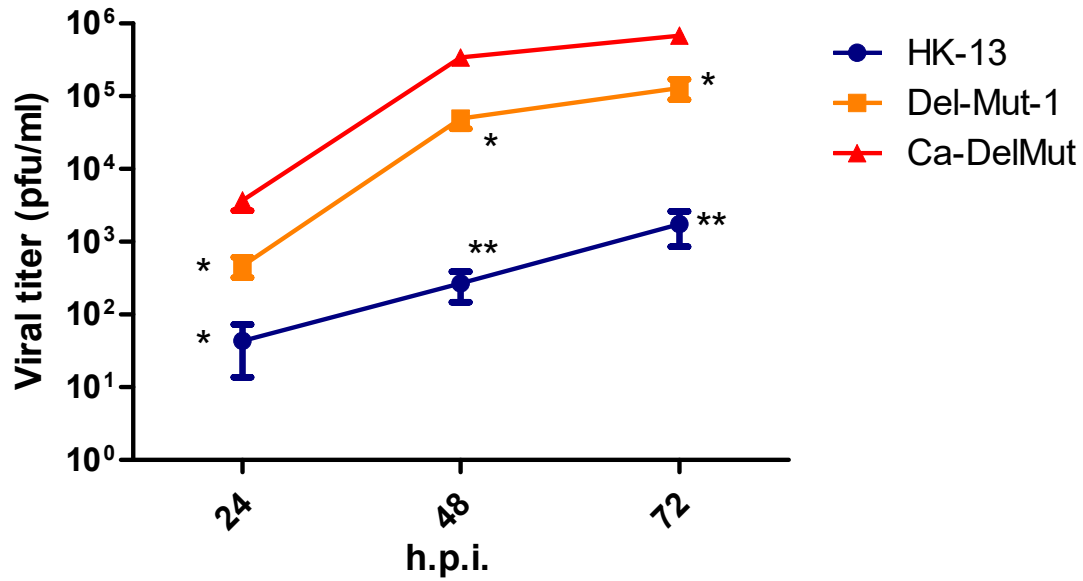
#### Deletion and mutations in Ca-DelMut virus genome compared to Wuhan-Hu-1

Nucleotide coordinate	Wuhan-Hu-1	Ca-DelMut			
		Nucleotide	Amino acid	Protein	ORF
1663	C	T	No change	NSP2	ORF1a
4455	C	T	A578V	NSP3a	ORF1a
8782	C	T	No change	NSP4	ORF1a
21636	C	T	P25L	S	S
22661	G	T	V367F	S	S
23598-23627	No deletion	30-base-pair deletion	10 aa deletion	S	S
24034	C	T	No change	S	S
26303	T	C	F20S	E	E
26729	T	C	No change	M	M
28077	G	C	V62L	ORF8	ORF8
28144	T	C	L84S	ORF8	ORF8

\*Details of deletion and mutations in the Ca-DelMut variant with reference to the Wuhan-Hu-1 SARS-CoV-2 strain (Wu et al., 2020)

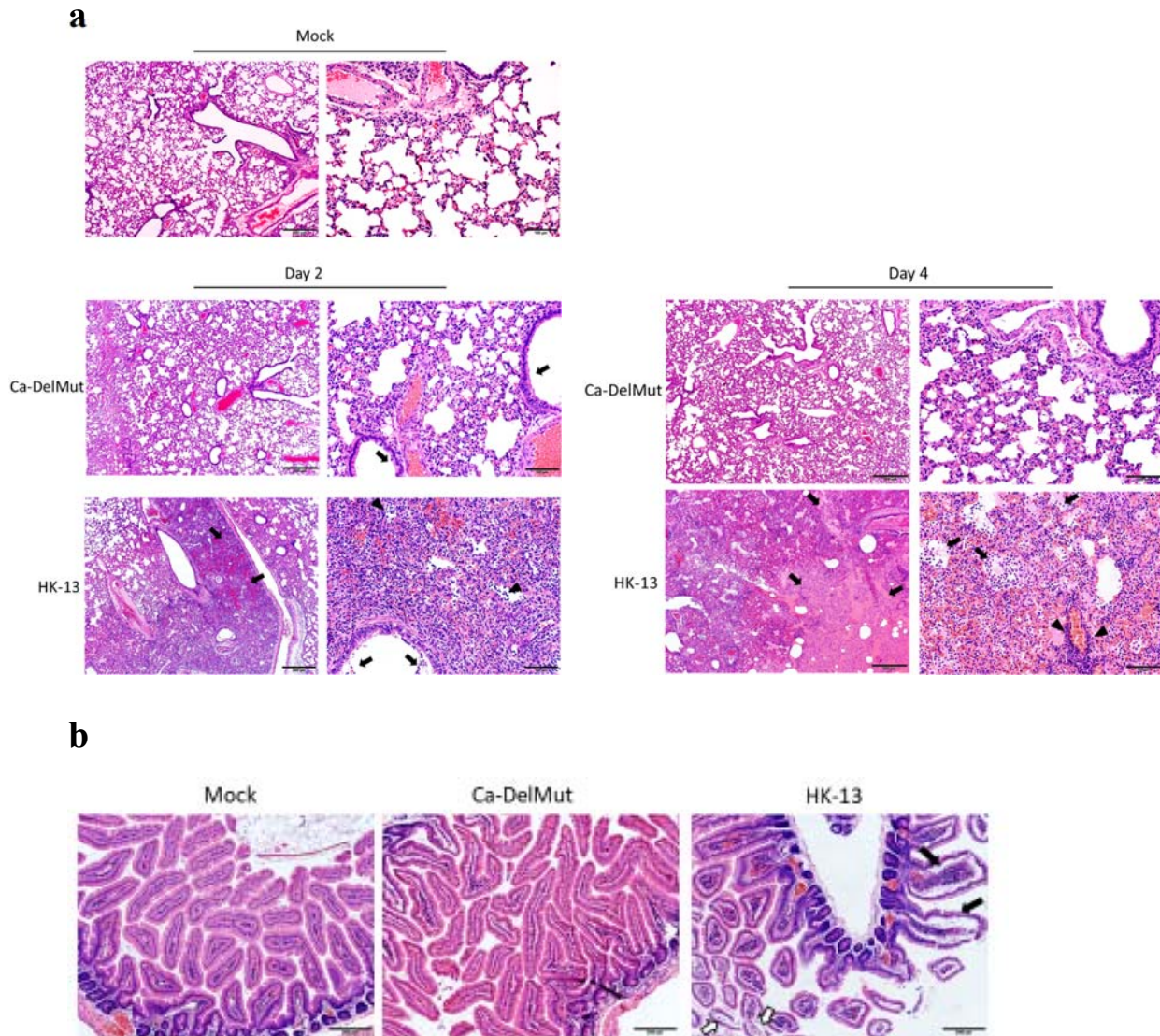
Wu, F., Zhao, S., Yu, B., Chen, Y.M., Wang, W., Song, Z.G., Hu, Y., Tao, Z.W., Tian, J.H., Pei, Y.Y., *et al.* (2020). A new coronavirus associated with human respiratory disease in China. *Nature* 579, 265-269.

Figure S1



**Figure S1.** Ca-DelMut exhibits a cold-adapted phenotype *in vitro*. Vero E6 cells were infected with Ca-DelMut and other viruses at 0.01 moi and incubated at 30°C. At the indicated time points, supernatants were collected and virus titer determined by plaque assay. Error bars represent mean ± s.d. (n=3). h.p.i.: hours post infection.

## Figure S2



**Figure S2.** Infection with Ca-DelMut causes only mild pathological changes. Hamsters were infected with  $1 \times 10^3$  pfu of either Ca-DelMut or HK-13 (WT), or mock infected. At days 2 and 4 post-infection, lungs and small intestine were collected and fixed in 10% formalin, and then processed into paraffin blocks and sections H&E stained.

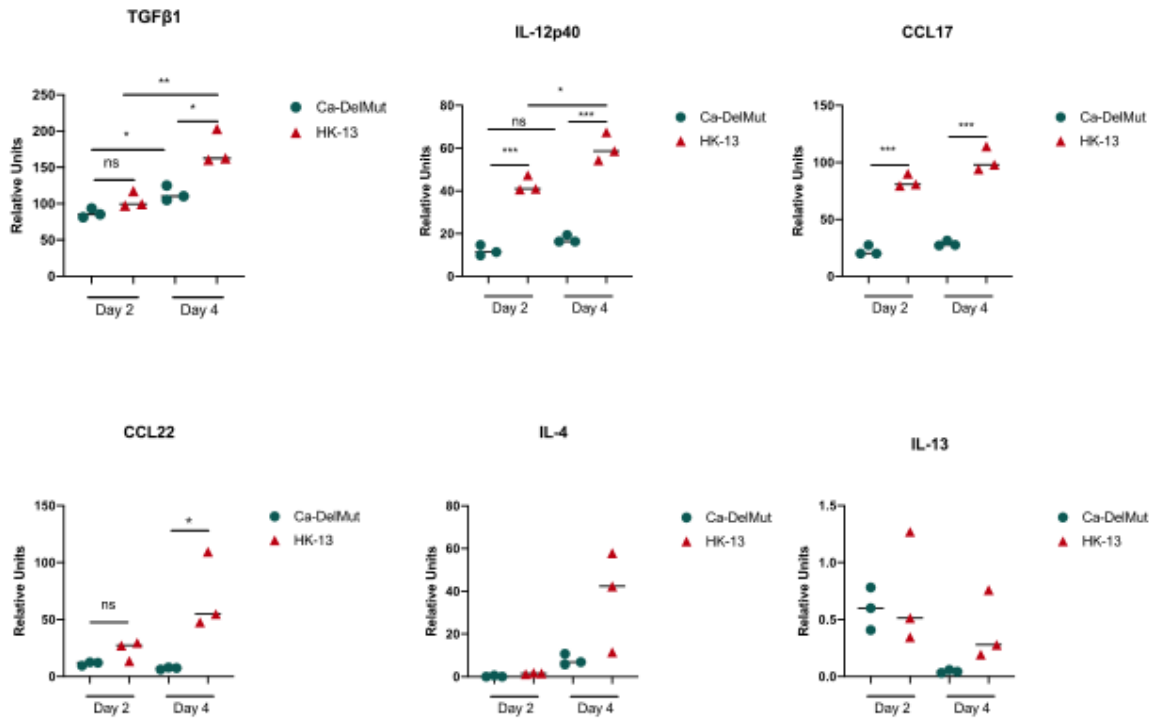
(a) The top panel shows normal lung structures in the lungs of mock-infected control hamsters at 4x (left) and 20x (right) magnification. At day 2 after infection with Ca-DelMut, lung tissues showed only mild regional alveolar septal infiltration and blood vessel congestion. No obvious bronchiolar epithelium desquamation or luminal debris (arrows), and no alveolar space infiltration or exudation were observed. At day 4, no deleterious progression of histopathology was observed.

For WT virus at day 2 post-infection, the low magnification image (left) showed regional lung consolidation and focal pulmonary hemorrhage (arrows). The higher magnification image

(right) showed massive alveolar space infiltration (arrowheads) and hemorrhage, with a little bronchiolar luminal cell debris (arrows) visible. At day 4 post WT<sub>2</sub>-infection, the low magnification image (left) showed intensive alveolar exudation, infiltration and hemorrhage resulting in pulmonary consolidation (arrows), while the higher magnification image (right) showed intensive protein rich exudates filling the alveolar space (arrows), in addition to massive infiltration and alveolar hemorrhage; a blood vessel shows moderate infiltration (arrowheads).

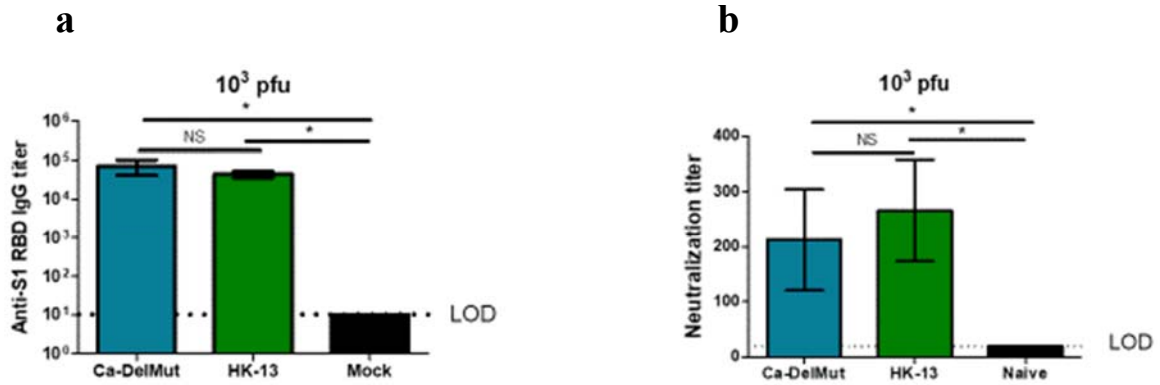
(b) Representative histological images of hamster small intestines. The left-most image shows mock-infected control hamster small intestinal villi with normal structure. At day 4 post infection with Ca-DelMut, no apparent histopathological changes were detected in the small intestine (middle). For WT virus infection, small intestinal lamina propria blood vessel congestion, infiltration and edema resulting in swelling of the villi (solid arrows) and enterocyte desquamation (open arrows) were observed.

Figure S3



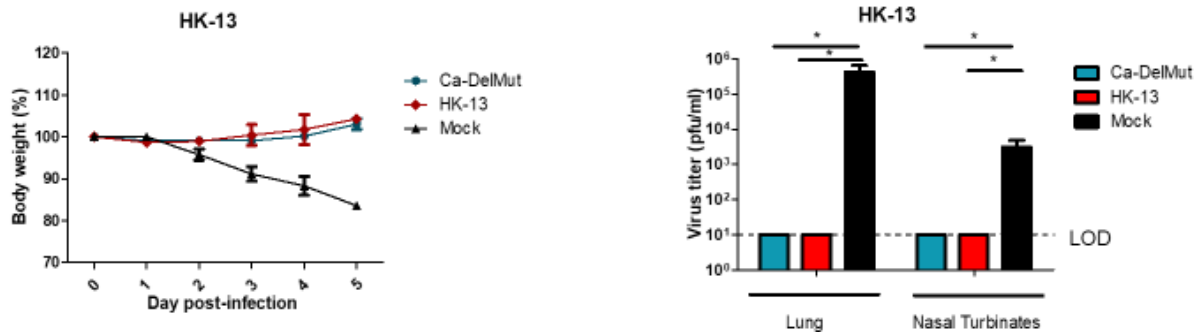
**Figure S3.** Ca-DelMut does not induce elevated levels of proinflammatory cytokines in hamsters. Hamsters were infected intranasally with  $1 \times 10^3$  pfu of either Ca-DelMut or WT HK-13 virus. At days 2 and 4, RNA was extracted from lung and nasal turbinate tissues using RNAsol RT procedures. cDNA was synthesized using oligo dT primers. Expression of different proinflammatory cytokines was examined by qPCR, normalized to the internal reference gene (hamster  $\gamma$ -actin), and the comparative Ct ( $2^{-\Delta\Delta Ct}$ ) method was utilized to calculate the cytokine expression profile. Statistical comparisons between means were performed by Student's t-test: \*\*\*  $p < 0.001$ , \*\*  $p < 0.01$ , \*  $p < 0.05$ , ns: not significant.

Figure S4



**Figure S4.** Lower dose ( $10^3$  pfu) Ca-DelMut immunization is able to induce a strong humoral response in hamsters. Hamsters were infected intranasally with  $1 \times 10^3$  pfu of either Ca-DelMut or HK-13 virus, or mock immunized. At day 21, blood was collected from hamsters and tested for anti-S1 RBD IgG titers (a) and neutralization activity against HK-13 virus (b). Error bars represent mean  $\pm$  s.d. ( $n=3$ ). LOD: level of detection.

**Figure S5**



**Figure S5.** Lower dose Ca-DelMut immunization still provides complete protection against WT HK-13 virus. Hamsters were infected intranasally with  $1 \times 10^3$  pfu of either Ca-DelMut or HK-13 virus, or mock immunized. At day 28 after immunization, hamsters were challenged with  $1 \times 10^3$  pfu of HK-13 virus. Body weight change and disease symptoms were monitored for 5 days. At day 5 post-infection, lungs and nasal turbinate tissues were collected for virus titration. Error bars represent mean  $\pm$  s.d. ( $n=3$ ).



**Figure S6**

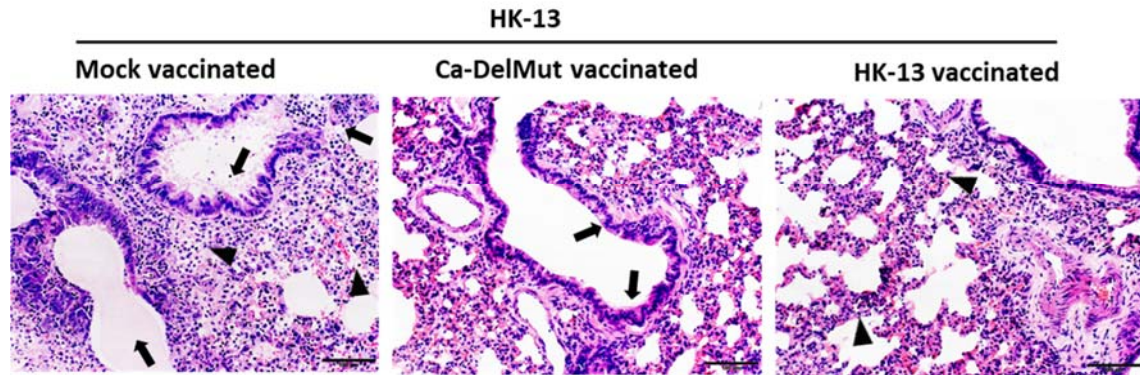


Figure S6. Low inoculum of Ca-DelMut provides protection against reinfection of wild type SARS-CoV-2. Hamsters were infected intranasally with  $1 \times 10^3$  pfu of either Ca-DelMut, HK-13 strain or mock immunized. At day 28 after immunization, hamsters were challenged with  $1 \times 10^3$  pfu of HK-13 virus. At day 5 post infection, lungs were collected for histopathological study. Lungs were fixed in 10% formalin, and then processed in paraffin blocks and H&E staining. Mock vaccinated hamster lung showed bronchiolar epithelial cells death and luminal secretion mixed with cell debris (arrows); diffuse alveolar infiltration and exudation (arrowheads); Ca-DelMut immunized lung showed no apparent bronchiolar epithelium cell death (arrows), alveoli showed regional septal infiltration. In HK-13 strain immunized hamster lung showed no apparent histopathology other than alveolar wall thickening (arrowheads) after re-challenge.